Electronic Supplementary Material (ESI) for Physical Chemistry Chemical Physics

Reaction Kinetics of CO_2 Absorption of Phosphonium Based Anion-Functionalized Ionic Liquids

*Burcu E. Gurkan, Thomas R. Gohndrone, Mark J. McCready, Joan F. Brennecke**

Department of Chemical and Biomolecular Engineering, University of Notre Dame, IN, 46556

Supplementary Information

I. Confirmation of tetraglyme being inert during CO_2 absorption reaction of ILs

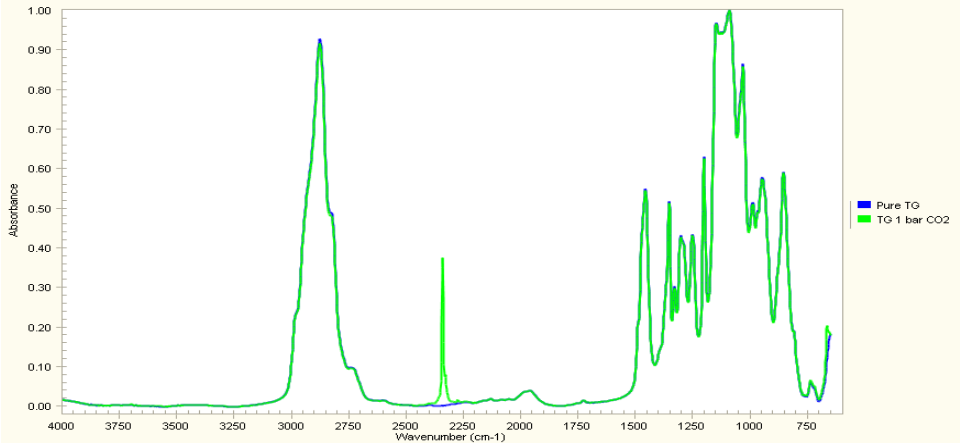

Fig S. 1 IR spectra of neat tetraglyme with (green) and without (blue) CO_2

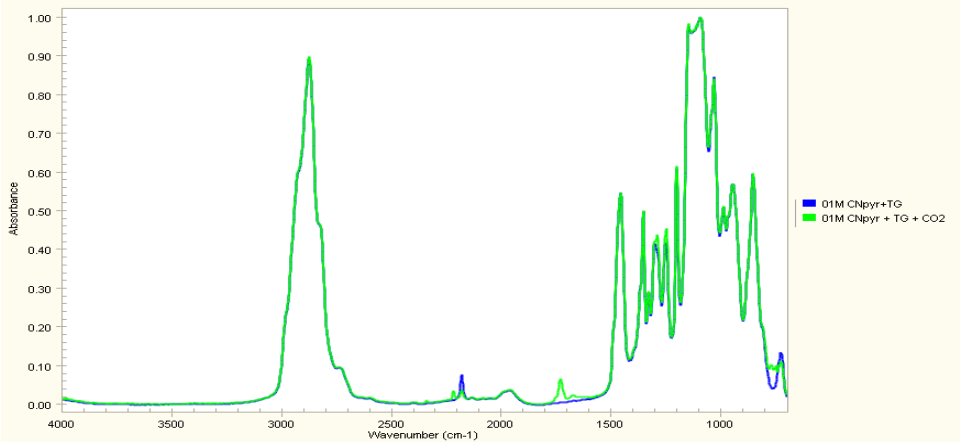

Fig S. 2 IR spectra of neat 0.1 M $[P_{66614}][2\text{-CNpyr}]$ in tetraglyme with (green) and without (blue) CO_2

* jfb@nd.edu

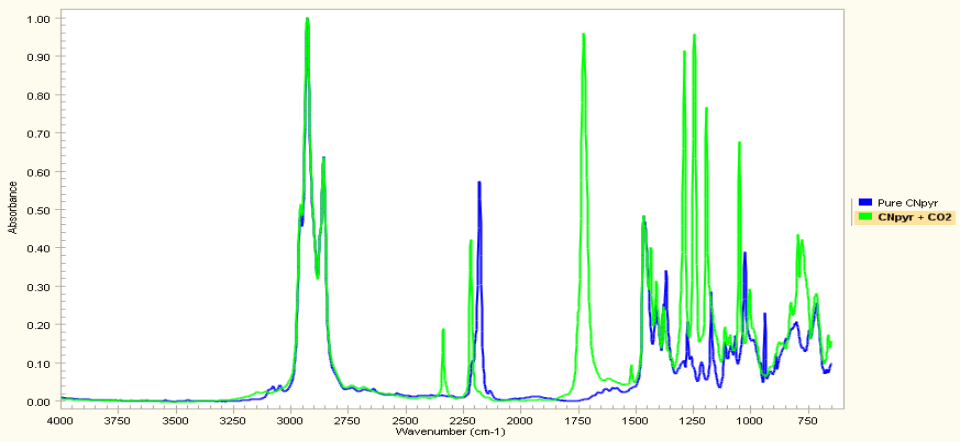

Fig S. 3 IR spectra of neat [P_{66614}][2-CNpyr] with (green) and without (blue) CO_2

The IR spectrum between 700 and 4000 cm^{-1} shown in Fig S.1 is observed for tetraglyme before and after it is exposed to CO_2. The only additional peak observed upon CO_2 addition is the physically dissolved CO_2 that appears between 2300 and 2400 cm^{-1}. In the presence of ionic liquid, (e.g. 0.1 M [P_{66614}][2-CNpyr]), two additional peaks appear around 1700 cm^{-1} (C=O stretch of reaction product between CO_2 and IL) and the peak around 2200 cm^{-1} (CN of the cyanopyrrolide) shifts to higher wavenumbers, as seen in Fig S.2. The physically dissolved CO_2 peak in this case is not observable since these IL/TG+CO_2 reaction measurements were done at very low CO_2 pressures. These changes observed in Fig S.2 are identical to those obtained for the pure IL reacting with CO_2, as shown in Fig. S.3. Because the solution is very dilute in IL, the characteristic peaks for the IL and CO_2 reaction in Fig. S.2 are observed to be weak in intensity. The additional peaks between 1100 and 1300 cm^{-1} from the IL + CO_2 reaction are not observed in Fig S.1 since the neat tetraglyme has very strong peaks that overlap and dominate in this region.

II. Reactor design and the details of the experimental methods:

The schematics shown in Fig S.4 detail the design of the reactor used for both kinetic and gas solubility measurements. The typical CO_2 pressure drop observed in the supply vessel during a kinetic run to maintain a constant pressure in the reactor is shown in Fig S.5.

Physico-chemical properties are either measured or estimated using appropriate approximations. The validation of the method employed in this study for the measurement of gas solubilities is shown in Table S.1. The CO_2 solubility in [hmim][Tf_2N] is measured and compared with the literature. The raw data measured at 10 and 25 °C are given in Table S.2. For the diffusivity of CO_2, the correlation (eqn. 16) adapted from the literature is used. The review of literature and the applicability of the correlation are provided in Table S.3 and Fig S.6, respectively.

Materials illustrating the discussions of the in-situ IR observations during the kinetic runs, fit of the activation energies and the details of the calculation of the desorption rates are provided at the end of this section.

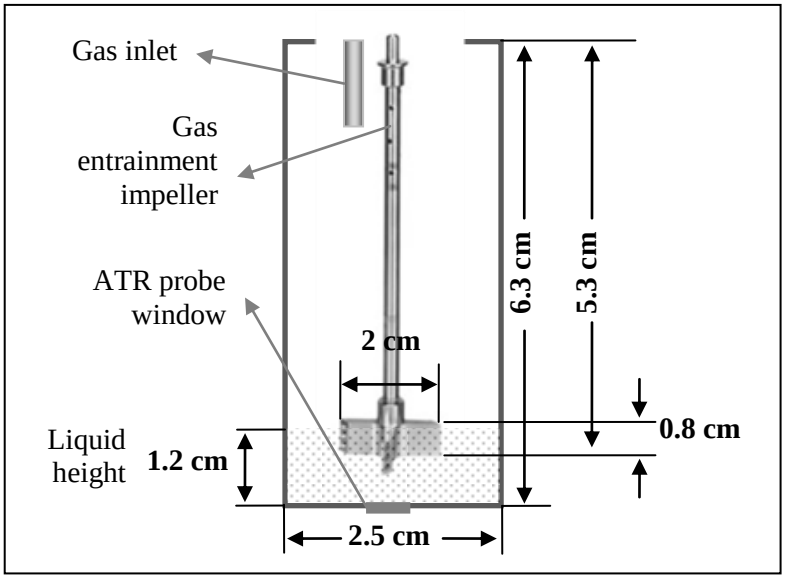

Fig S. 4 Schematics of IR-reactor showing the stirrer location in the liquid

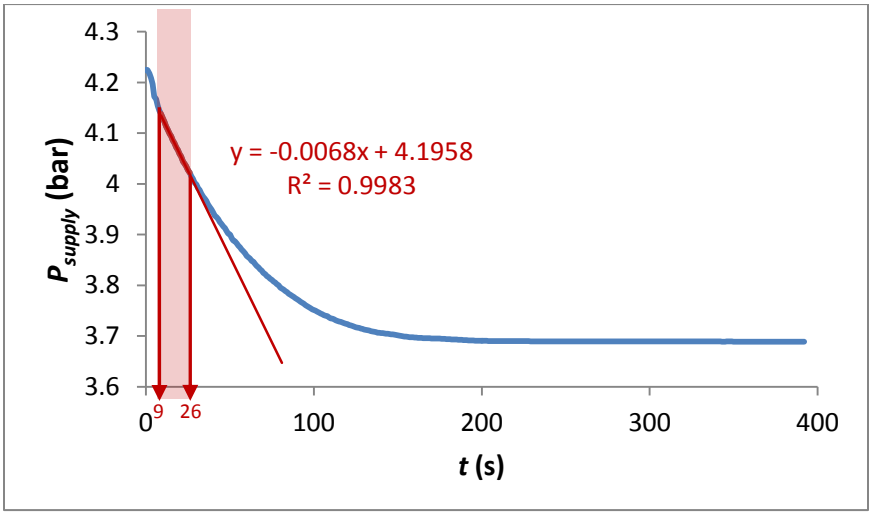

Fig S. 5 Observed pressure drop in the supply vessel during a typical rate experiment. The average flux is calculated from the slope of the linear line fitted to the selected highlighted interval. Data collected for the 0.1M $[P_{66614}][Pro]$ / TG system at 22 °C is shown.

Table S. 1 Comparison of measured and literature Henry's Law constants, *H*, for CO_2 in [hmim][Tf_2N] at 10 and 25 °C

	10 °C	25 °C
H (bar) this study	25	33
H (bar) literature [1]	24.2	31.6
% difference	3.3	4.4

Table S. 2 CO_2 solubility of [hmim][Tf_2N] at 10 and 25 °C measured in this study

P (bar)	T (°C)	x_{CO2}	P (bar)	T (°C)	x_{CO2}
0.850	25.2	0.0261	0.471	10	0.020
1.560	25.3	0.0482	0.527	10	0.022
2.510	25.1	0.0767	0.801	10	0.033
0.186	25.3	0.0054	0.935	10	0.038
0.519	25.1	0.0156	1.100	10	0.045
1.147	25.3	0.0346	1.220	10.1	0.050
1.567	25.2	0.0472	1.459	10	0.060
1.986	25.1	0.0591	1.650	10.1	0.067
--	--	--	1.734	10.1	0.071
--	--	--	1.998	10.1	0.081

Table S. 3 Comparison of experimental and predicted (using eqn. 15) CO_2 diffusivities for some organics and ILs. The highlighted compounds are the ones that fall beyond the applicable range of the correlation provided in eqn. 15 and the ones that display special interactions such as water and ethylene glycol.

	T (° C)	molar volume (L/mol)	viscosity (cP)	diffusion coefficient x10^6 (cm^2/s)	D_{CO2} predicted	% error
water [2]	*25*	*0.018*	*0.8903*	*19.25*	*38.28*	*99*
water [3]	*20*	*0.018*	*1.002*	*15.0*	*36.21*	*141*
ethylene glycol [4]	*25*	*0.056*	*16*	*2.79*	*9.85*	*253*
ethanol [5]	25	0.063	1.2	34.20	33.27	-3
isobutyl alcohol [5]	25	0.073	3.36	22.00	20.50	-7
toluene [6 7]	25	0.118	0.552	40.25	47.92	19
heptane[5]	25	0.146	0.411	60.30	55.04	-9
hexadecane [6]	50	0.301	2.04	22.10	25.92	17
[emim][TfO] [8]	30	0.192	45	5.20	6.06	16
[bmim][BF_4] [9]	30	0.189 [10]	75	4.10	4.76	16
[bmim][BF_4] [11]	**30**	**0.189 [10]**	**75**	**1.14**	**4.76**	**318**

Table S.3 Continued

	T (° C)	molar volume (L/mol)	viscosity (cP)	diffusion coefficient x10^6 (cm^2/s)	D_{CO2} predicted	% error
[bmim][PF_6] [8]	30	0.211	176	2.70	3.19	18
[bmim][PF_6] [11]	**30**	**0.211**	**176**	**0.8**	**3.19**	**297**
[desmim][TfO] [8]	*30*	*0.210*	*554*	*1.10*	*1.86*	*69*
[emim][Tf_2N] [8]	30	0.258	26	6.60	7.84	19
[pmmim][Tf_2N] [9]	30	0.288 [12]	66.6	5.60	5.04	-10
[N_{1114}][Tf_2N] [13]	30	0.290	71	4.87	4.89	0
[bmim][Tf_2N] [9]	30	0.292 [12]	37.4	8.50	6.61	-22
[bmim][BETI] [8]	30	0.294	77	4.50	4.71	5
[bmpy][Tf_2N] [9]	30	0.306	51	6.00	5.71	-5
[N_{1134}][Tf_2N] [13]	30	0.315	85	4.83	4.49	-7
[P_{2444}][DEP] [14]	30	0.323	207	3.50	2.96	-16
[N_{1116}][Tf_2N] [13]	30	0.325	100	4.38	4.16	-5
[N_{1136}][Tf_2N] [13]	30	0.353	126	3.72	3.73	0
[N_{2226}][Tf_2N] [13]	30	0.366	167	4.68	3.27	-30
[N_{4441}][Tf_2N] [13]	*30*	*0.384*	*386*	*3.41*	*2.21*	*-35*
[N_{11110}][Tf_2N] [13]	30	0.393	173	4.60	3.22	-30
[N_{11310}][Tf_2N] [13]	30	0.425	183	3.78	3.13	-17
[P_{66614}][DCA] [14]	30	0.578	213	3.00	2.92	-3
[thtdp][Cl] [8]	*30*	*0.590*	*919*	*2.20*	*1.47*	*-33*
[P_{66614}][Cl] [14]	*30*	*0.590*	*1316*	*3.00*	*1.24*	*-59*
[N_{1888}][Tf_2N] [13]	*30*	*0.601*	*532*	*3.43*	*1.90*	*-45*
[emim][$EtSO_4$] [15]	*30*	*0.641*	*76*	*2.19*	*4.73*	*116*
[P_{66614}][DBS] [14]	*30*	*0.731*	*3011*	*1.70*	*0.84*	*-51*
[P_{66614}][Tf_2N] [14]	*30*	*0.804*	*243*	*6.20*	*2.74*	*-56*

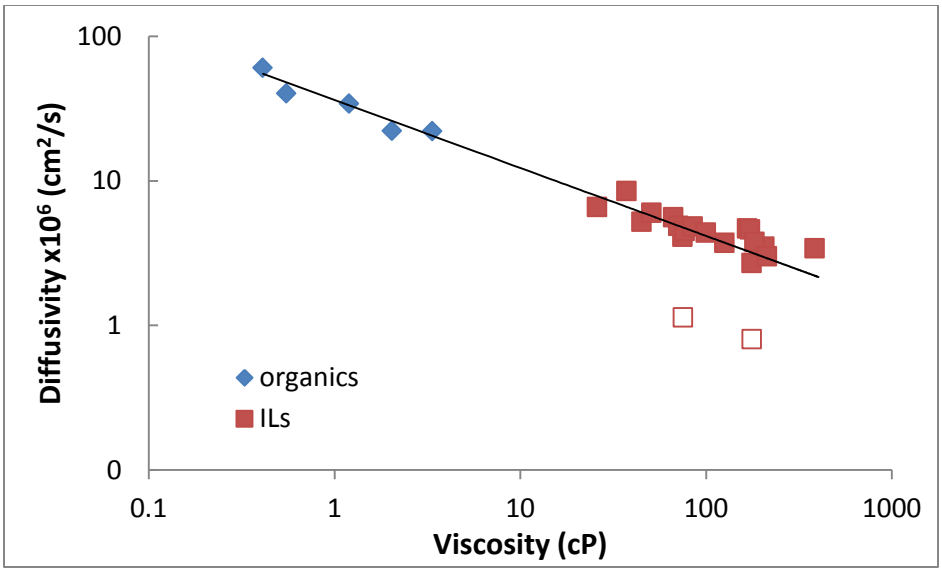

Fig S. 6 Correlation between diffusivity of CO_2 and the viscosity of organics. The correlation is extrapolated to higher viscosities and the experimental CO_2 diffusivities measured for ILs fall on this line with a maximum of 35 % error, including $[N_{4441}][Tf_2N]$. The diffusivities obtained by Shiflett and Yokozeki [11] are represented with open symbols. ILs with molar volumes above 0.59 L/mol and viscosities above 386 cP are excluded.

Table S. 4 First order reaction rate constants measured for $[P_{66614}][Pro]$ / TG solutions

C_{IL} (mol / L)	run #	P_{CO2} (mbar)	T (°C)	k (1/s)	$k_{average}$ (1/s)
0.05	1	10.6	21.2	1100	1000
	2	14.2	21.4	990	
	3	14.1	21.8	980	
0.1	1	15.1	22.6	1800	1900
	2	14.8	21.7	2200	
	3	15.6	22.2	1800	
0.15	1	14.9	22.2	4000	4200
	2	15.0	22.1	4300	
	3	14.7	22.2	4500	
0.1	1	16.4	29.9	4300	4400
	2	16.4	30.0	4300	
	3	16.2	29.8	4500	
0.1	1	16.9	39.8	5900	6200
	2	16.2	39.5	6200	
	3	16.1	39.6	6500	
0.1	1	17.1	49.8	8000	8600
	2	17.0	49.4	8600	
	3	16.7	49.6	9100	
0.1	1	15.9	60.0	11100	11000
	2	18.2	60.0	9600	
	3	17.3	60.8	12100	

Table S. 5 First order reaction rate constants measured for $[P_{66614}][2\text{-CNpyr}]$ / TG solutions

C_{IL} (mol / L)	run #	P_{CO2} (mbar)	T (°C)	k (1/s)	$k_{average}$ (1/s)
0.05	1	15.4	21.8	390	370
	2	15.1	21.9	370	
	3	15.0	23.0	340	
0.1	1	16.2	22.5	790	850
	2	14.9	21.1	880	
	3	14.8	22.1	870	
0.15	1	15.2	21.6	1600	1500
	2	15.2	21.9	1500	
	3	14.6	21.1	1300	
0.1	1	16.0	30.0	910	910
	2	16.0	29.9	940	
	3	16.5	29.9	890	
0.1	1	11.6	39.8	1000	1100
	2	15.4	39.8	1100	
	3	16.6	39.8	1100	
0.1	1	14.7	49.5	1200	1200
	2	15.6	49.1	1300	
	3	16.1	49.7	1200	
0.1	1	14.2	59.5	1300	1600
	2	16.9	59.7	1700	
	3	16.1	59.5	1400	

Table S. 6 First order reaction rate constants measured for $[P_{66614}][3\text{-}CF_3\text{pyra}]$ / TG solutions

C_{IL} (mol / L)	run #	P_{CO2} (mbar)	T (°C)	k (1/s)	$k_{average}$ (1/s)
0.05	1	15.4	22.6	160	150
	2	15.4	22.0	140	
	3	15.4	23.2	140	
0.1	1	15.5	22.0	320	320
	2	15.7	22.6	300	
	3	15.1	22.7	330	
0.15	1	15.0	22.3	530	500
	2	15.2	21.3	490	
	3	15.4	23.2	490	
0.1	1	16.4	29.9	320	340
	2	16.7	29.9	340	
	3	15.3	29.9	350	
0.1	1	14.3	39.7	510	490
	2	16.9	39.9	490	
	3	17.1	39.9	470	
0.1	1	17.5	49.3	560	530
	2	16.9	50.0	500	
	3	16.3	49.0	520	
	4	16.4	48.4	550	
0.1	1	15.1	58.8	740	740

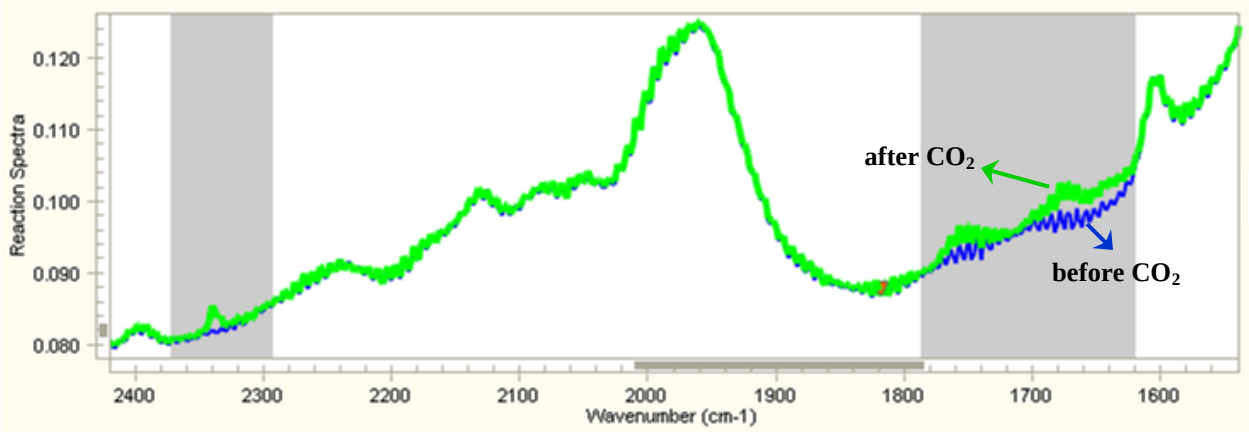

Fig S. 7 IR spectra of 0.1M [P_{66614}][3-CF_3pyra] / TG at 60 °C before and after reaction with CO_2. Highlighted regions (2370 – 2310) cm^{-1} and (1780 – 1620) cm^{-1} correspond to the dissolved CO_2 and the newly formed -COO^- peaks, respectively.

The in-situ IR observations during kinetic measurements helped determine the conditions where the pseudo first order approximation was valid and select the time interval for kinetic analysis. Fig S.7 illustrates the observed absorbance between 2400 and 1500 cm^{-1} for 0.1 M [P_{66614}][3-CF_3pyra] at 60 °C. Due to the low CO_2 capacity of this IL, the changes in the IR spectrum are small. In other words, this is a 'worst-case scenario. In order to clearly see the changes, the selected interval is expanded in Fig S.7, which causes the spectra to appear noisy. The CO_2 and newly formed –COO^- peaks are highlighted in the figure.

Table S. 7 Arrhenius parameters fitted to the kinetic data shown in Figure 5. R^2 indicates the goodness of the fit

$k = A \cdot exp\left(\frac{-E_a}{RT}\right)$	***Ea* (kJ/mol)**	***A***	**R^2**
[P_{66614}][Pro]	43 ± 7	8.02 x 10^8	0.9475
[P_{66614}][2-CNpyr]	11 ± 6	0.73 x 10^3	0.8876
[P_{66614}][3-CF_3pyra]	18 ± 4	4.65 x 10^3	0.9523

On the desorption rates:

CO_2 absorption r_{abs} and desorption r_{des} rate expressions can be written as

$$r_{abs} = k_2 C_{IL} C_{CO2} \quad (S.1)$$

$$r_{des} = k_{-1} C_{IL-CO2} \quad (S.2)$$

and

$$\frac{r_{des}}{r_{abs}} = \frac{k_{-1} C_{IL-CO2}}{k_2 C_{IL} C_{CO2}} = \frac{k_{-1} n_{IL-CO2}}{k_2 n_{IL} n_{CO2}} V_{sample} \quad (S.3)$$

where the moles of species i can be written in terms of their mole fraction: $n_i = x_i n_{total}$. Furthermore, the amount of CO_2 that is available to react with the IL can be written in terms of the Henry's Law constant ($P_{CO2} = H\, x_{CO2}$).

$$\frac{r_{des}}{r_{abs}} = \frac{k_{-1} x_{IL-CO2}}{k_2 x_{IL} P_{CO2}} \frac{V_{sample}}{n_{total}} H \qquad \text{(S.4)}$$

When we write the overall reaction between CO_2 and IL to form IL-CO_2

$$CO_{2\,(g)} + IL_{\,(l)} \leftrightarrow \text{IL-}CO_{2\,(l)}$$

with forward and reverse rate constants as k_2 and k_{-1}, respectively, we can write the equilibrium constant for this reaction as

$$K = \left(\frac{\hat{f}_{CO2}}{f^0_{CO2}}\right)^{-1} \left(\frac{\hat{f}_{IL}}{f^0_{IL}}\right)^{-1} \left(\frac{\hat{f}_{IL-CO2}}{f^0_{IL-CO2}}\right)^{1} \qquad \text{(S.5)}$$

Assuming the standard state as 1 bar ($f^0_{CO2} = 1$) and the fugacity of the pure liquid at the same temperature as the system (f^0_{IL} and f^0_{IL-CO2}) to be the vapor pressures of those pure components, eqn. (S.5) can be simplified as

$$K = \frac{(x_{IL-CO2}\gamma_{IL-CO2})}{(y_{CO2}P_{CO2})(x_{IL}\gamma_{IL})} \qquad \text{(S.6)}$$

where $\gamma_i$is the activity coefficient and x_i is the mole fraction. Because the IL or the IL/tetraglyme mixture is essentially nonvolatile, the only specie present in the gas phase is CO_2. Therefore, the mole fraction of CO_2 in the gas phase is 1 (y_{CO2}=1). When we further assume that the activity coefficients of the IL and that of the product are similar, eqn. (S.6) can be simplified to:

$$K = \frac{(x_{IL-CO2})}{(P_{CO2})(x_{IL})} \qquad \text{(S.7)}$$

Returning to eqn. (S.4), the left hand side includes the familiar expression of the equilibrium constant derived in eqn. (S.7). At chemical equilibrium absorption and desorption rates are equal. Therefore,

$$1 = \frac{k_{-1}}{k_2} K \frac{V_{sample}}{n_{total}} H \qquad \text{(S.8)}$$

Rearranging eqn. (S.8) in terms of the desorption rate constant (s^{-1}) yields:

$$k_{-1} = \frac{k_2}{K} \frac{1}{H} \frac{n_{total}}{V_{sample}} \qquad \text{(S.9)}$$

The temperature dependence of the equilibrium constant is shown in Fig S.8 (data for $[P_{66614}]$[2-CNpyr] and $[P_{66614}]$[3-CF_3pyra] are given in Table 4 and those for $[P_{66614}]$[Pro] can be found in Goodrich, 2011 [16]). The slope of ln$K$ vs $1/T$ yields the reaction enthalpy in the form of $(-\Delta H/R)$ where R is the gas constant. The intercept corresponds to the change of entropy in the form of $(\Delta S/R)$. Accordingly, the reaction enthalpies of CO_2 absorption by $[P_{66614}]$[Pro] and $[P_{66614}]$[2-CNpyr] are -44 and -43 kJ / mol, respectively. Comparing the CO_2 isotherms for $[P_{66614}]$[Pro] in [17] with that of $[P_{66614}]$[2-CNpyr] in [18], it is clear that the reaction enthalpies for both ILs should be quite different. $[P_{66614}]$[Pro] has a higher affinity towards CO_2. Therefore, one would expect the reaction enthalpy for this IL to be more exothermic. The only explanation for this unexpected

enthalpy is that the assumed Langmuir-type model is not suitable to describe the CO_2 reaction with $[P_{66614}][Pro]$.

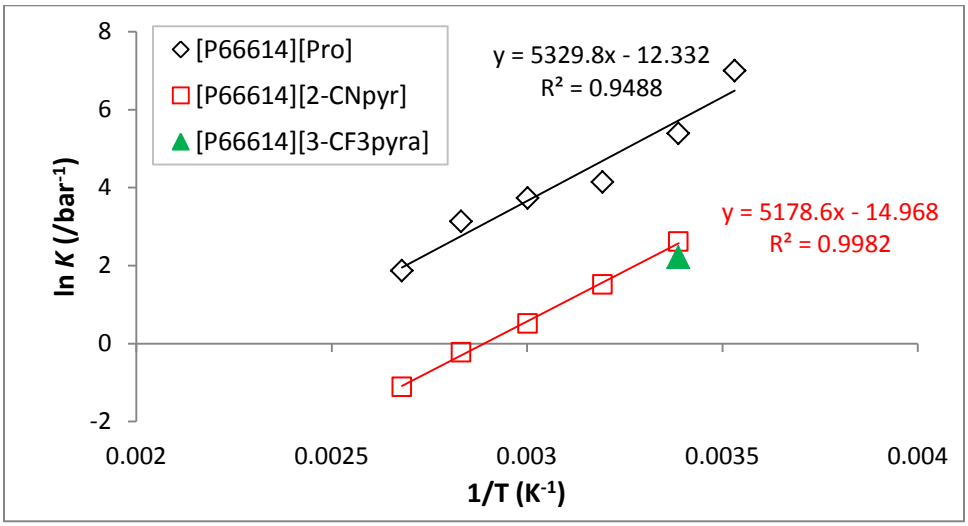

Fig S. 8 Dependence of the equilibrium constants for reaction of CO_2 with $[P_{66614}][Pro]$ and $[P_{66614}][2\text{-CNpyr}]$ on temperature.

To calculate the equilibrium constants at 80 and 100 °C, where data is not available, the relations obtained in Fig S.8 were used. It was assumed that temperature dependence of ΔH is negligible. For $[P_{66614}][3\text{-}CF_3\text{pyra}]$, the same change of entropy for $[P_{66614}][2\text{-CNpyr}]$ ($\Delta S = -130$ kJ / mol) was adapted to calculate the reaction enthalpy.

III. Other raw data for the measured properties:

Table S. 5 Experimental densities for the neat tetraglyme (TG) and IL/TG solutions. Kodama et al. [19]. reported an uncertainty of ±0.0001 g·cm^{-3} for their density measurement of TG; however, they did not report the water content of their sample. The discrepancy between our measurements and those reported by Kodama et al. can be explained by the difference in water content.

		density (g/cm^3)							
C_{IL} (mol/L)	water content (ppm)	22^{0}C	25^{0}C	30^{0}C	35^{0}C	40^{0}C	45^{0}C	50^{0}C	60^{0}C
		[P_{66614}][Pro]							
0.05	400	1.00568	1.00295	0.99841	0.99387	0.98936	0.9848	0.98029	0.97123
0.10	473	1.00289	1.00021	0.99571	0.99125	0.98675	0.98227	0.97782	0.96882
0.15	550	0.99989	0.99724	0.99281	0.98838	0.98398	0.97956	0.97514	0.9663
		[P_{66614}][2-CNpyr]							
0.05	470	1.00575	1.00304	0.9985	0.99398	0.98944	0.98488	0.98037	0.97132
0.10	477	1.00213	0.99945	0.99497	0.99049	0.98602	0.98162	0.9771	0.9682
0.15	490	0.99858	0.99596	0.99153	0.98712	0.98273	0.97831	0.97393	0.96514
		[P_{66614}][3-CF_3pyra]							
0.05	358	1.0071	1.00438	0.99984	0.99529	0.99073	0.98616	0.98163	0.97254
0.10	378	1.00501	1.00231	0.9978	0.9933	0.98882	0.98433	0.97983	0.9708
0.15	400	1.00298	1.00033	0.99587	0.99144	0.98698	0.98255	0.9781	0.96922
		tetraglyme							
this work	224	1.00890	1.00618	1.00160	0.99700	0.99245	0.98786	0.98327	0.97409
[19] Kodama et al., 2011			1.00743	1.00281		0.99356		0.98432	0.97507

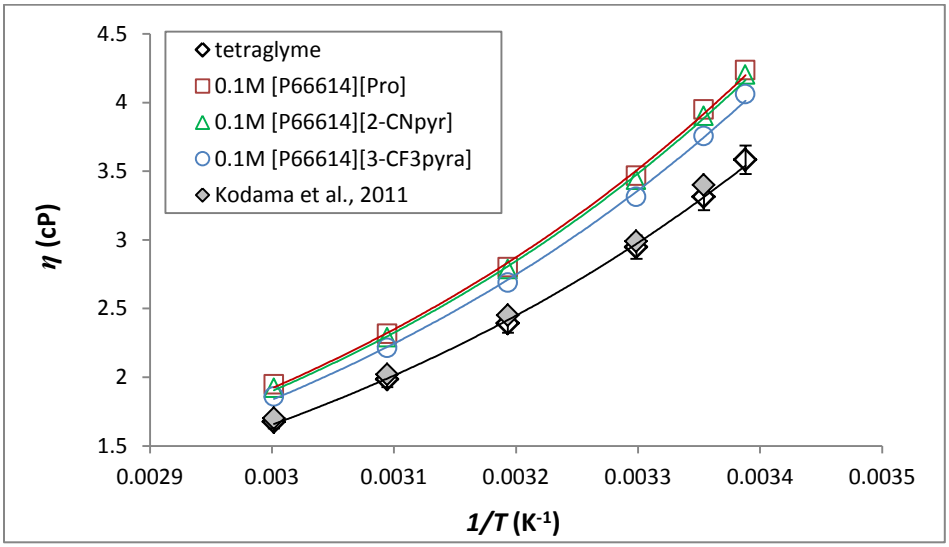

Fig S. 9 Arrhenius behavior of viscosities of tetraglyme and 0.1M IL / TG solutions. The lines represent fitted exponential trends.

Table S. 4 Data measured for the CO_2 solubility in tetraglyme.

P (bar)	T (°C)	x_{CO2}	P (bar)	T (°C)	x_{CO2}
0.381	22.1	0.0132	*0.149*	*23.5*	*0.005*
0.649	22.3	0.0225	0.272	24	0.0091
0.877	22.1	0.0308	0.385	24.2	0.0129
1.1	22.1	0.0388	0.69	24.4	0.0246
1.379	22.2	0.0483	0.976	24.2	0.0331
1.671	22.2	0.0581	1.76	24.2	0.0588
2.007	22.2	0.071	2.2	24.3	0.0725
2.277	22.2	0.08	2.941	24.6	0.0942
2.579	22.3	0.0905	3.906	24.8	0.1223
2.905	22.3	0.101	4.784	25.3	0.1521
0.382	21.9	0.0132	0.465	25	0.0153
0.838	22.1	0.0288	0.747	25.1	0.0249
1.167	22.2	0.0399	1.036	25	0.0349
1.493	22.3	0.0509	1.587	24.9	0.0538
1.854	22.2	0.0632	--	--	--
2.157	22.3	0.0733	--	--	--
2.926	22.3	0.0973	--	--	--
0.395	30.3	0.011	*0.162*	*38.9*	*0.0039*
0.602	30.3	0.0166	0.285	39.1	0.007
0.801	30.3	0.0221	0.397	39.1	0.0099
1.014	30.4	0.0279	0.51	39	0.0127
1.195	30.5	0.0328	0.938	39	0.0234
1.361	30.7	0.0373	1.857	39	0.0451
1.558	30.4	0.043	2.87	38.9	0.0719
1.776	30.4	0.0489	4.64	38.8	0.1137
2.072	30.4	0.0567	0.463	39.2	0.01
2.811	30.4	0.0756	0.488	39.4	0.0102
--	--	--	1.021	39.4	0.0224
--	--	--	1.401	39.6	0.0314
--	--	--	2.063	39.5	0.0466
--	--	--	3.173	39.5	0.0717
0.349	49.8	0.0064	0.255	59.5	0.0043
0.596	49.6	0.0114	0.392	59.6	0.0067
0.822	49.5	0.0157	0.504	59.6	0.0089
1.033	49.5	0.0201	0.617	59.3	0.0108
1.248	49.5	0.0251	0.727	59.3	0.0127
1.55	49.6	0.0316	0.836	59.2	0.0145
1.875	49.7	0.0382	1.031	59.1	0.0178
2.196	49.6	0.045	1.244	59	0.0214
2.617	49.7	0.0533	1.543	59.1	0.027
0.349	50.6	0.0063	2.108	59.1	0.0369
0.59	50.3	0.0109	3.161	59	0.0552
0.814	49.8	0.0154	0.604	59.1	0.0099
1.031	49.9	0.0201	0.962	58.9	0.0163
1.24	50	0.0253	1.158	58.9	0.0199
1.79	50	0.0372	1.726	59.1	0.0296
2.249	50	0.0474	2.325	59	0.0398
2.678	49.9	0.0582	3.09	59.1	0.0529

Table S. 5 N_2O solubility in tetraglyme measured in this study.

P (bar)	T (°C)	x_{N2O}	P (bar)	T (°C)	x_{N2O}
0.507	22.4	0.0112	0.432	39.5	0.0079
0.859	22.5	0.0204	0.606	39.4	0.0113
1.108	22.3	0.0273	0.812	39.4	0.0156
1.335	22.2	0.0335	1.027	39.4	0.02
1.556	22.3	0.0394	1.249	39.5	0.0252
1.814	22.2	0.0464	1.539	39.4	0.0318
2.064	22.2	0.054	1.862	39.4	0.0387
2.303	22.2	0.0608	3.384	39.3	0.0683
2.537	22.2	0.0669	0.436	39.8	0.0086
3.143	22.2	0.0826	0.871	39.7	0.0174
3.709	22.2	0.098	1.174	39.7	0.0242
4.04	22.3	0.1073	1.58	39.7	0.0336
0.48	22.1	0.0128	1.964	39.7	0.0429
0.854	22.2	0.0227	2.211	39.7	0.0505
1.23	22.4	0.0329	2.783	39.7	0.0648
1.607	22.2	0.0433	0.625	59	0.009
2.109	22.3	0.0565	1.004	58.9	0.0146
2.479	22.4	0.0666	1.243	59.1	0.019
3.248	22.4	0.087	1.649	59.1	0.0256
0.203	24.8	0.0052	2.054	59.1	0.0338
0.828	24.9	0.021	2.329	59	0.0388
1.148	25.1	0.0295	3.013	59	0.0493
1.599	25	0.0409	0.462	59.4	0.0066
2.066	25.15	0.0525	0.532	59.5	0.0075
2.841	25.23	0.0712	0.811	59.4	0.0117
--	--	--	1.04	58.9	0.0151
--	--	--	1.17	59.3	0.0173
--	--	--	1.372	59.3	0.0206
--	--	--	1.588	59.3	0.0239
--	--	--	1.71	58.9	0.0298
--	--	--	2.092	59	0.035
--	--	--	2.434	58.9	0.0399
--	--	--	3.12	58.8	0.0495

Table S. 6 Data measured for N_2O solubility in [hmim][Tf_2N] and [hmpy][Tf_2N]

[hmim][Tf_2N]			[hmpy][Tf_2N]		
P (bar)	T (°C)	x_{N2O}	P (bar)	T (°C)	x_{N2O}
0.187	24.8	0.006	0.154	24.9	0.005
0.429	24.8	0.014	0.34	25	0.012
0.803	24.9	0.031	0.591	24.9	0.02
1.035	24.9	0.038	0.838	25	0.029
1.277	25	0.046	1.045	25	0.037
1.367	25	0.049	1.437	24.9	0.052
0.146	25	0.004	1.792	24.9	0.064
0.272	25	0.008	0.113	49.7	0.002
0.5	25	0.016	0.272	49.7	0.006
0.831	25.1	0.027	0.4	50.1	0.008
1.244	25	0.041	0.523	50.1	0.011
1.854	25	0.061	0.876	50	0.019
1.289	25.1	0.044	1.243	50	0.028
0.105	50	0.002	1.612	50	0.036
0.332	50.1	0.006	1.866	50.1	0.043
0.642	50.1	0.013			
1	50.1	0.021			
1.201	50.1	0.026			
1.421	50.2	0.031			
1.93	50.2	0.043			

Table S. 7 Data measured for N_2O solubility in [P_{66614}][Pro]

P (bar)	T (°C)	x_{N2O}	P (bar)	T (°C)	x_{N2O}
0.097	24.7	0.004	0.145	25.2	0.006
0.287	24.8	0.013	0.338	25.1	0.015
0.499	24.8	0.023	0.588	25.1	0.026
0.61	24.8	0.032	0.869	25	0.040
0.804	24.8	0.040	1.086	25	0.047
0.935	24.9	0.046	--	--	--
1.106	24.9	0.055	--	--	--
1.236	24.9	0.061	--	--	--

REFERENCES

1. J. L. Anderson, J. K. Dixon, E. J. Maginn and J. F. Brennecke, *Journal of Physical Chemistry B*, 2006, **110**, 15059-15062.
2. G. F. Versteeg and W. P. M. Vanswaaij, *Journal of Chemical and Engineering Data*, 1988, **33**, 29-34.
3. J. H. Arnold, *Journal of the American Chemical Society*, 1930, **52**, 3937-3955.
4. W. Hayduk and V. K. Malik, *Journal of Chemical and Engineering Data*, 1971, **16**, 143-&.
5. G. A. Davies, A. B. Ponter and K. Craine, *Canadian Journal of Chemical Engineering*, 1967, **45**, 372-&.
6. W. Hayduk and S. C. Cheng, *Chemical Engineering Science*, 1971, **26**, 635-&.
7. W. J. McManamey and J. M. Woollen, *Aiche Journal*, 1973, **19**, 667-669.
8. D. Morgan, L. Ferguson and P. Scovazzo, *Industrial & Engineering Chemistry Research*, 2005, **44**, 4815-4823.
9. Y. Hou and R. E. Baltus, *Industrial & Engineering Chemistry Research*, 2007, **46**, 8166-8175.
10. J. Jacquemin, M. F. C. Gomes, P. Husson and V. Majer, *Journal of Chemical Thermodynamics*, 2006, **38**, 490-502.
11. M. B. Shiflett and A. Yokozeki, *Industrial & Engineering Chemistry Research*, 2005, **44**, 4453-4464.
12. C. P. Fredlake, J. M. Crosthwaite, D. G. Hert, S. Aki and J. F. Brennecke, *Journal of Chemical and Engineering Data*, 2004, **49**, 954-964.
13. R. Condemarin and P. Scovazzo, *Chemical Engineering Journal*, 2009, **147**, 51-57.
14. L. Ferguson and P. Scovazzo, *Industrial & Engineering Chemistry Research*, 2007, **46**, 1369-1374.
15. A. H. Jalili, A. Mehdizadeh, M. Shokouhi, A. N. Ahmadi, M. Hosseini-Jenab and F. Fateminassab, *Journal of Chemical Thermodynamics*, 2010, **42**, 1298-1303.
16. B. Goodrich, M.S, Thesis in *Department of Chemical and Biomolecular Engineering*, University of Notre Dame, Notre Dame, IN, 2011.
17. B. E. Gurkan, J. C. de la Fuente, E. M. Mindrup, L. E. Ficke, B. F. Goodrich, E. A. Price, W. F. Schneider and J. F. Brennecke, *Journal of the American Chemical Society*, 2010, **132**, 2116-+.
18. B. Gurkan, B. F. Goodrich, E. M. Mindrup, L. E. Ficke, M. Massel, S. Seo, T. P. Senftle, H. Wu, M. F. Glaser, J. K. Shah, E. J. Maginn, J. F. Brennecke and W. F. Schneider, *Journal of Physical Chemistry Letters*, 2010, **1**, 3494-3499.
19. D. Kodama, M. Kanakubo, M. Kokubo, S. Hashimoto, H. Nanjo and M. Kato, *Fluid Phase Equilib.*, 2011, **302**, 103-108.